# {110}-exposed rutile titanium dioxide nanorods in photocatalytic performance†

Tsung-Ying Ke,[a] Chih-Wei Peng,[ce] Chi-Young Lee,*[ab] Hsin-Tien Chiu[c] and Hwo-Shuenn Sheu[d]

*Received 3rd February 2009, Accepted 20th April 2009*
*First published as an Advance Article on the web 11th May 2009*
**DOI: 10.1039/b902299f**



Single crystalline rutile $TiO_2$ nanorods were prepared by reacting sodium titanate with hydrochloric acid. The proposed formation mechanism involves a growth pathway. The growth proceeds along [001], and the circumferential faces are {110}, which are identified as the photoactive faces of rutile titanium dioxide. Both the heterogeneous (photocatalyst only) and the combined heterogeneous/homogeneous (photocatalyst and $H_2O_2$) photocatalytic performances support its activity. The mechanism of formation and photocatalytic property are extensively studied.

## Introduction

Titanium dioxide is an important metal oxide because it scatters light strongly; has a high dielectric constant; is non-toxic and is chemically inert. In addition to its well-known use as a pigment, titanium dioxide has recently been adopted as a photocatalyst[1] of the degradation of organic pollutants under UV irradiation, as a material for use in solar cells,[2,3] in gas sensors and in lithium ion batteries;[4,5] it is also employed as a catalyst support.[6,7]

Among various AOPs (advanced oxidation processes),[8–12] $H_2O_2$ is commonly employed as an electron and hole scavenger to prevent their recombination, and also as a source of radicals, such as produced in the photo Fenton reaction of Fe ions with $H_2O_2$. However, metal ions will represent another form of pollution. Replacing metal ions with a solid photocatalyst to generate excitons is environmentally friendly. Also, the greater absorption cross-section of $TiO_2$ particles than of iron ions corresponds to the more efficient utilization of light. Some research has been conducted, that when rutile $TiO_2$ was used as a photocatalyst, the degradation efficiency of pollutants enhanced several to tens of times as $H_2O_2$ was added to the reaction solution, while when using anatase $TiO_2$ as a photocatalyst, the degradation efficiency enhanced little by $H_2O_2$ addition.[13,14]

Rutile is the most stable form of titanium dioxide[15,16] on the macroscopic scale and is formed at high temperatures.[17] In recent times, the synthesis of rutile nanorods has been commonly described, but the growth mechanism is rarely elucidated.[18–20] This investigation describes the preparation of rutile nanorods with the [001] wire axis and {110} circumferential faces, by reacting sodium titanate with acid solution at low temperature and ambient pressure. The growth mechanism is examined experimentally. The effect of the surfaces on the photocatalytic performance is also examined extensively.

## Experimental

### 2.1. Preparation of nanorod rutile titanium dioxide

Nanorods of rutile titanium dioxide were prepared by treating sodium titanate with acid, as follows.[21] First, anatase $TiO_2$ (Aldrich) was refluxed in 10M NaOH solution at 150 °C until all $TiO_2$ had transformed into sodium titanate. After the unreacted NaOH had been removed by filtration and then washed, the sodium titanate was separated into two parts. One part (1 g) was refluxed in 100 mL 1 M HCl (at pH 0) at 150 °C. The other (1 g) was refluxed in 100 mL 10 M HCl (at pH $\ll$ 0) in the presence of 5 M NaCl at 150 °C. After reaction for 3 d, the collected powders were immersed in 10 M NaOH solution at room temperature for 1 h, washed, and dried under a vacuum. They were characterized by XRD, ESCA, BET, SEM and TEM.

### 2.2 Purification of commercial rutile titanium dioxide

To study the properties of pure rutile, the anatase phase was chemically separated from the commercial rutile (Aldrich) and P25 (particles with 25% rutile and a diameter of *ca* 30 nm) using HF solution. The commercial samples were immersed in 10% HF for 24 h to remove the anatase phase. The collected powders were immersed in 10 M NaOH solution at room temperature for 1 h, which removed the surface F ions (ESI†). After they had been immersed, washed and dried, pure rutile in the form of particles was obtained with the same size as the initial $TiO_2$ powder. The samples of commercial rutile and P25 are called micro- and nano-sized rutile, respectively.

### 2.3 Photocatalytic experiment

The photocatalytic performances of rutile $TiO_2$ nanorods, micro-sized particles, and nano-sized particles were studied. The as-prepared rutile nanorods were further treated with alkali solution

[a]*Department of Materials Science and Engineering, National Tsing Hua University, Hsinchu, Taiwan, 30043, R. O. C. E-mail: cylee@mx.nthu.edu.tw*
[b]*Center for Nanotechnology, Materials Science, and Microsystems, National Tsing Hua University, Hsinchu, Taiwan, 30043, R. O. C*
[c]*Department of Applied Chemistry, National Chiao Tung University, Hsinchu, Taiwan, 30050, R. O. C*
[d]*National Synchrotron Radiation Research Center, 101 Hsin-Ann Road, Hsinchu Science Park, Hsinchu, 30077, Taiwan, R.O.C*
[e]*Institut des Matériaux Jean Rouxel, LPC, 2 rue de la Houssinière, BP 32229, 44322 Nantes Cedex 3, France*

† Electronic supplementary information (ESI) available: Additional experimental details. See DOI: 10.1039/b902299f

to remove Cl from their surfaces. They were then illuminated under Xe light at an intensity of about 1 W $cm^{-2}$. The powder was placed in 0.25 mM Methylene Blue solution, stirred in the dark for 1 h, and then illuminated. During illumination, a trace amount of solution was removed every 5 min and centrifuged, before being filtered through a Millipore filter to separate the $TiO_2$ particles. UV-VIS spectra of the filtrates were obtained to determine the concentration of Methylene Blue. $H_2O_2$ was added to a concentration of 10 mM.

## Results and discussion

The SEM images show that the powder obtained by treating titanate with 1 M HCl consists of uniformly sized shuttle-like bundles with diameters of about 50 nm and lengths of 200∼400 nm, as presented in Fig. 1a The energy dispersive X-ray spectrum (EDX) of the product indicates the presence of Ti and O only, but the ESCA analysis reveals a little Cl in the powder. After they had been treated with NaOH solution, the nanorod bundles comprised only Ti and O, according to ESCA analysis. XRD was adopted to characterize structurally the obtained products (ESI†). The patterns indicate major reflections at $2\theta$ values of 27.5, 36.3 and 41.4°, corresponding to reflections from the (110), (101) and (111) lattice planes of $TiO_2$ rutile, respectively.

Fig. 1b presents a low-magnification transition electron microscopic image (TEM) of an isolated rutile nanorod bundle, which has around ten inseparable nanorods with diameters of about 10 nm and lengths of hundreds of nanometers. The SAED in Fig. 1d presents a spot pattern in the region that is indicated in Fig. 1b, revealing the single crystalline nature of the samples. The patterns can be indexed as the [1-10] zone axis of rutile $TiO_2$. The pattern indicates that the apparent growth direction of the nanorods is [001]. Fig. 1c presents an HRTEM image of the region that is marked in Fig. 1b, and the fringes from the {001} and {110} planes, revealing *d* spacings of 0.296 and 0.324 nm, respectively. The {110} planes are parallel to the rod axis, while the {001} planes are parallel to the cross-section of the rods. Theoretically, the dihedral angle of the tetragonal structure of the {001} and {110} planes is 90°. According to the literature, the nanorod cross-section is rectangular,[22] suggesting that the circumferential faces of the nanorods are {110} planes, which are posited to be the most stable faces. In addition, when acid concentration was increased to 10 M, the more acidic environment promoted both axial and sideway growth, and micro-sized agglomerates with nanorod bundles obtaied (ESI).†

Furthermore, when NaCl was added to the acidic solution, the obtained powder comprised nanorods with a declined diameter of *ca* 5 nm and increased aspect ratio, as presented in Fig. 2a and b. Fig. 2d presents the corresponding SAED of the area shown in Fig. 2c. Figs. 2c and d indicate that the very thin nanorods with the [001] growth direction and {110} revealing surfaces are similar to the thick nanorods.

In 1995, Cheng[23] prepared fibrillar rutile by the hydrothermal approach using $TiCl_4$ as the reagent in the concentrated mineral acid medium. In 2005, Zhu and Gao[24] prepared a thin rod-like rutile from H-titanate in aqueous concentrated acid, in which H-titanate resolved into detached $TiO_6$ octahedrons or small clusters, and then restacked as thin rod-like rutile; this process is also thought to be a build-up process. HRTEM and ED show that the fiber axis is along the [001] direction.

Sugimoto[25] investigated the solution chemistry of $Ti(OH)_n(H_2O)_{6-n}^{(4-n)+}$ ($n = 0\sim4$) complexes, and identified different $Ti^{4+}$ ion species $-Ti(OH)_4(OH_2)_2$, $Ti(OH)_3(OH_2)_3^+$, $Ti(OH)_2(OH_2)_4^{2+}$, $Ti(OH)(OH_2)_5^{3+}$ and $Ti(OH_2)_6^{4+}$—in aqueous

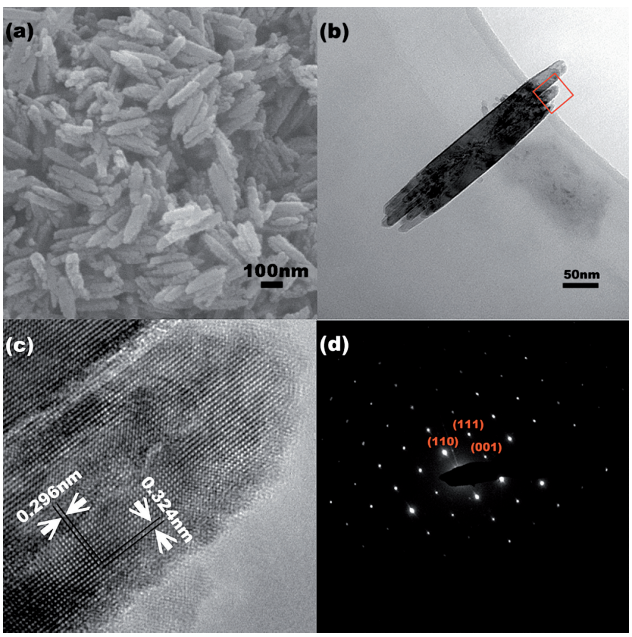


**Fig. 1** EM of rutile nanorods obtained by acidic treatment of sodium titanate in 1 M HCl. (a) SEM image of rutile nanorods. (b) TEM image of single rutile nanorod bundle. (c) HRTEM of tip of bundle. (d) ED of tip of bundle.

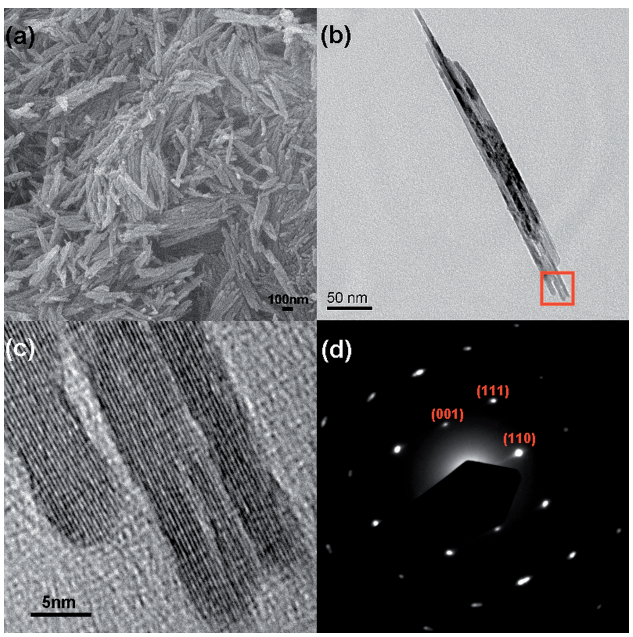


**Fig. 2** EM of rutile nanorods obtained by acidic treatment of sodium titanate in 10 M HCl in presence of 5 M NaCl. (a) SEM image of rutile nanorods. (b) TEM image of single rutile nanorod bundle. (c) HRTEM and (d) ED of tip of the bundle.

 

solutions. The dominant species varies with the pH of the solution. For example, at pH > 7, $Ti(OH)_4(OH_2)_2$ dominates, but when pH < 0, $Ti(OH)_2(OH_2)_4^{2+}$ dominates. Hence, the $Ti^{4+}$ ion is surrounded by at least four $H_2O$ ligands in concentrated acid solution (pH < 0). Fibril rutiles precipitate out of the acidic solution at pH < 0, while anatase particles can be obtained in dilute acidic and alkaline solutions.

According to the literature[23–32] and the observations herein, $Ti(OH)_2(OH_2)_4^{2+}$, $Ti(OH)(OH_2)_5^{3+}$ and $Ti(OH_2)_6^{4+}$ may be built-up to produce fibril rutile, while $Ti(OH)_3(OH_2)_3^{+}$ and $Ti(OH)_4(OH_2)_2$ are the building blocks of particle anatase. In rutile, each $TiO_6$ octahedron shares two opposing edges—each with an adjacent neighbor in a linear chain structure. These chains lie in alternating directions to yield sheets of $TiO_2$ and three-dimensional rutile can be formed by the stacking of such sheets. During condensation in an acid-catalyzed sol-gel process, the attacking group donates its pair of electrons to the $Ti^{4+}$ ion center to produce a Ti–O bond, and $H_2O$ and $H^+$ are the leaving groups. The acid-catalyzed condensation process for forming the Ti–O–Ti bond is as follows.

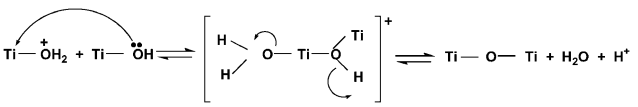


Fig. 3 presents the process of stacking isolated $TiO_6$ by condensation. The two stacking pathways are designated Path 1 and Path 2. On Path 1, condensation proceeds in the equatorial plane of the octahedrons, resulting in growth by edge sharing in the <001> directions, elongating these directions of the rutile titanium dioxide. On Path 2, condensation occurs at the axial apex of the octahedrons, and growth proceeds by the sharing of corners in the <110> directions, enlarging the {001} planes of the rutile. Since ligand $H_2O$ that preferentially bonds to the center metal in the equatorial position is a better leaving group than $OH^-$, the condensation between $H_2O$ and $OH^-$ proceeds rapidly in the equatorial position, leading to oriented growth in the <001> direction. $OH^-$ preferentially occupies the apex position, making condensation in the <110> directions slow, forming fibril rutile. Once the <110> surface had formed in the acid solution, Cl ions adhered to part of the side surface, as revealed by ESCA, restricting sideways growth.

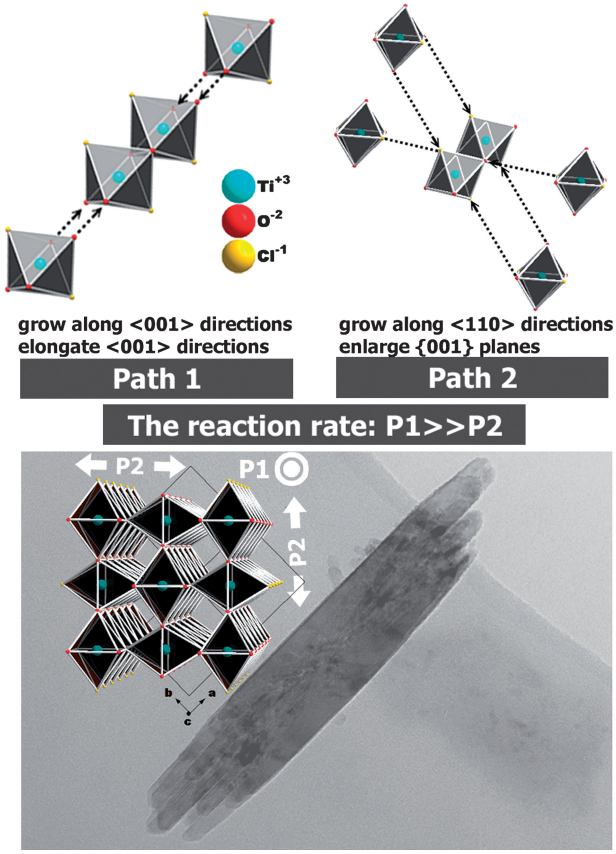


**Fig. 3** Structure and formation pathways of rutile nanorods.

To support this claim, the concentration of Cl ions was increased by adding NaCl. The growth in the <110> direction was further inhibited and the diameter thus decreased to *ca* 5 nm, as presented in Fig. 2. Fig. 2 also indicates that the prepared nanorods have the same growth direction, supporting the claimed growth mechanism. The photocatalytic behavior of the specially shaped rutile particles was also studied.

Fig. 4 presents the morphologies of nanorods, micro-sized rutiles, and nano-sized rutiles. Fig. 4a indicates that the rutile nanorod bundles comprise a few inseparable nanorods with diameters of about 50 nm and lengths of 200 nm. Although the sample that precipitated from a higher Cl ion concentration had a higher surface area (116 $m^2\ g^{-1}$) than rutile nanorods (68 $m^2/g$), according to BET measurements, its photocatalytic performance was almost the same as that of rutile nanorods, perhaps because of the aggregation of nanoparticles in solution, since these precipitated sample and rutile nanorods had very similar particle-size distributions in solution, and both aggregated to micro-size (ESI).† Fig. 4b presents micrometer-sized rutile particles with a mean diameter of about 0.1 μm obtained from purified commercial rutile. The nanometer-sized rutile particles, presented in Fig. 4c, have a diameter of about 30 nm. Fig. 5 presents the photocatalytic behavior of different rutiles in the degradation of Methylene Blue under irradiation by UV light. P25 with a size of about 30 nm was also tested for comparison. First, in the heterogeneous photocatalysis experiment (solid-line), without $H_2O_2$, although as-prepared rutile nanorods performed poorly as a photocatalyst (not shown), the rutile nanorods that had been washed in alkali solution to remove the Cl from the surface exhibited better photoactivity than that of other rutile particles, irrespective of their size. P25 performed excellently, as stated. The same findings were obtained from the heterogeneous/homogeneous photocatalysis experiment (dashed-line) which was performed in an $H_2O_2$ environment. The blank experiment, with $H_2O_2$ but no photocatalyst, exhibited almost no degradation of Methylene Blue, while combining rutile $TiO_2$ with $H_2O_2$ markedly improved photocatalytic performance. The rutile nanorods still outperformed all of the rutile samples. Adding 10 mM $H_2O_2$ enhanced the performance of all pure rutile samples by roughly the same magnitude, but that of P25 by only a little, because it contained little rutile. The photocatalytic performance was further improved by increasing the $H_2O_2$ concentration to over 1 M. Therefore, the nanorod bundles are proposed to have both an effective surface and suitable

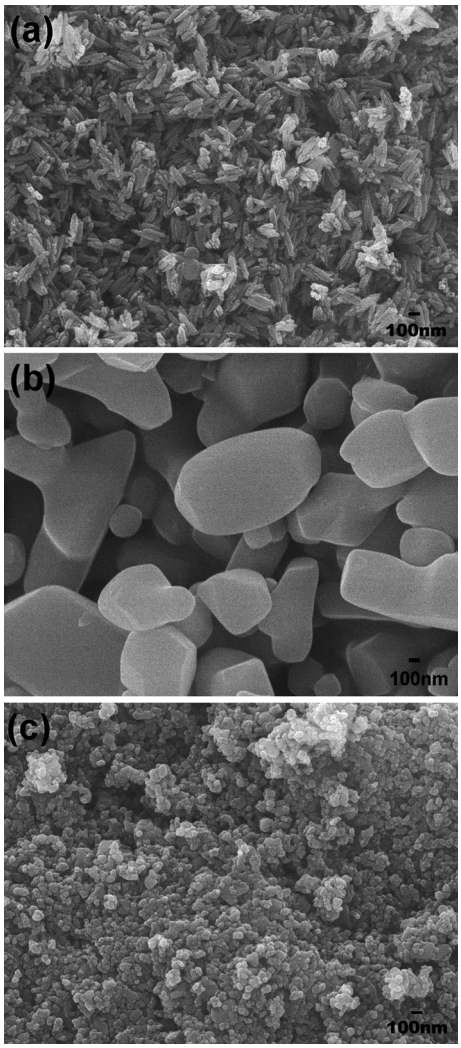


**Fig. 4** Morphologies of (a) rutile nanorods, (b) micro-sized rutile, and (c) nano-sized rutile. The scale bar is 100 nm.

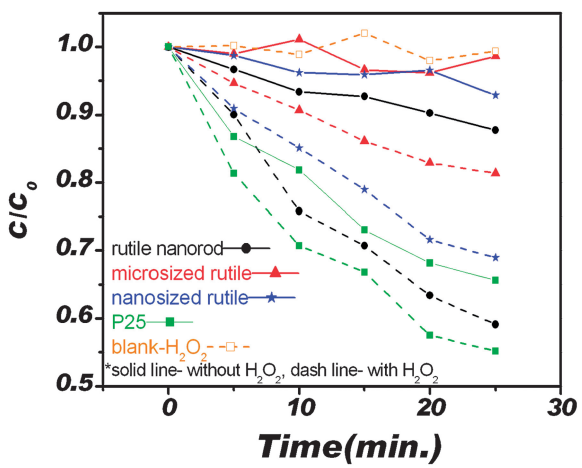


**Fig. 5** Photocatalytic performance of P25 and the three rutile samples, including rutile nanorod, microsized, and nanosized rutiles, with or without $H_2O_2$ addition. The blank one is the degradation of Methylene Blue in $H_2O_2$ solution, but no $TiO_2$ photocatalyst was added.

morphology for photocatalytic reactions. According to TEM, the nanorod bundles comprise nanorods with exposed {110} circumferential planes. This result indicates that the {110} planes of rutile $TiO_2$ are the photoactive surfaces.

## Conclusion

In summary, uniform rutile nanorods along the [001] axis with very large circumferential {110} faces were synthesized resulting from Cl ions adhering to the {110} surface, which leads to hindering the lateral growth of nanorods. Based on this mechanism, the diameter of the rutile nanorods was controlled by changing the concentration of Cl ions, and nanorods with higher aspect ratios thus obtained. Under UV illumination, the nanorods exhibited stronger photocatalysis than variously sized rutile particles, indicating the superior photocatalytic character of rutile {110} faces. Also, the especially made {110}-exposed rutile $TiO_2$ nanorods photocatalytically outperform other $TiO_2$ samples, including micro-sized and nano-sized rutile $TiO_2$ with or without $H_2O_2$ addition. This result may show that the green process, which uses the stable form $TiO_2$ (rutile) with an especially revealed surfaces, uses solar energy more efficiently.

## References

1 R. Wang, K. Hashimoto, A. Fujishima, M. Chikuni, E. Kojima, A. Kitamura, M. Shimohigoshi and T. Watanabe, *Nature*, 1997, **388**, 431–432.
2 B. Oregan and M. Gratzel, *Nature*, 1991, **353**, 737–740.
3 N. G. Park, J. van de Lagemaat and A. J. Frank, *J. Phys. Chem. B*, 2000, **104**, 8989–8994.
4 Y. S. Hu, L. Kienle, Y. G. Guo and J. Maier, *Adv. Mater.*, 2006, **18**, 1421–1426.
5 M. V. Koudriachova, N. M. Harrison and S. W. de Leeuw, *Phys. Rev. Lett.*, 2001, **86**, 1275–1278.
6 T. Ohno, K. Sarukawa and M. Matsumura, *New J. Chem.*, 2002, **26**, 1167–1170.
7 R. Zanella, S. Giorgio, C. H. Shin, C. R. Henry and C. Louis, *J. Catal.*, 2004, **222**, 357–367.
8 A. M. Nienow, J. C. Bezares-Cruz, I. C. Poyer, I. Hua and C. T. Jafvert, *Chemosphere*, 2008, **72**, 1700–1705.
9 A. Ozcan, Y. Sahin, A. S. Koparal and M. A. Oturan, *J. Electroanal. Chem.*, 2008, **616**, 71–78.
10 E. M. Siedlecka, W. Mrozik, Z. Kaczynski and P. Stepnowski, *J. Hazard. Mater.*, 2008, **154**, 893–900.
11 R. Andreozzi, V. Caprio, A. Insola and R. Marotta, *Catal. Today*, 1999, **53**, 51–59.
12 D. D. Dionysiou, M. T. Suidan, I. Baudin and J. M. Laine, *Appl. Catal., B*, 2004, **50**, 259–269.
13 J. G. Jia, T. Ohno and M. Matsumura, *Chem. Lett.*, 2000, 908–909.
14 T. Hirakawa, K. Yawata and Y. Nosaka, *Appl. Catal., A*, 2007, **325**, 105–111.
15 T. Torimoto, N. Nakamura, S. Ikeda and B. Ohtani, *Phys. Chem. Chem. Phys.*, 2002, **4**, 5910–5914.
16 U. Diebold, *Surf. Sci. Rep.*, 2003, **48**, 53–229.
17 S. Yoo, S. A. Akbar and K. H. Sandhage, *Adv. Mater.*, 2004, **16**, 260–264.
18 M. N. Tahir, P. Theato, P. Oberle, G. Melnyk, S. Faiss, U. Kolb, A. Janshoff, M. Stepputat and W. Tremel, *Langmuir*, 2006, **22**, 5209–5212.
19 S. Meuer, P. Oberle, P. Theato, W. Tremel and R. Zentel, *Adv. Mater.*, 2007, **19**, 2073–2078.
20 A. Dessombz, D. Chiche, P. Davidson, P. Panine, C. Chaneac and J. P. Jolivet, *J. Am. Chem. Soc.*, 2007, **129**, 5904–5909.
21 T. Kasuga, M. Hiramatsu, A. Hoson, T. Sekino and K. Niihara, *Langmuir*, 1998, **14**, 3160–3163.
22 E. Hosono, S. Fujihara, K. Kakiuchi and H. Imai, *J. Am. Chem. Soc.*, 2004, **126**, 7790–7791.

 

23 H. M. Cheng, J. M. Ma, Z. G. Zhao and L. M. Qi, *Chem. Mater.*, 1995, **7**, 663–671.
24 H. Y. Zhu, Y. Lan, X. P. Gao, S. P. Ringer, Z. F. Zheng, D. Y. Song and J. C. Zhao, *J. Am. Chem. Soc.*, 2005, **127**, 6730–6736.
25 T. Sugimoto, X. P. Zhou and A. Muramatsu, *J. Colloid Interface Sci.*, 2002, **252**, 339–346.
26 C. F. Baes, Jr. and R. E. Mesmer, *The Hydrolysis of Cations*, Wiley Interscience, New York, 1976.
27 W. W. Zhang, S. G. Chen, S. Q. Yu and Y. S. Yin, *J. Cryst. Growth*, 2007, **308**, 122–129.
28 Z. Ambrus, K. Mogyorosi, A. Szalai, T. Alapi, K. Demeter, A. Dombi and P. Sipos, *Appl. Catal., A*, 2008, **340**, 153–161.
29 N.-G. Park, J. van de Lagemaat and A. J. Frank, *J. Phys. Chem. B*, 2000, **104**, 8989–8994.
30 R. H. Chu, J. C. Yan, S. Y. Lian, Y. H. Wang, F. C. Yan and D. W. Chen, *Solid State Commun.*, 2004, **130**, 789–792.
31 S. Yin, R. X. Li, Q. L. He and Tsugio Sato, *Mater. Chem. Phys.*, 2002, **75**, 76–80.
32 S. Yin, H. Hasegawa and T. Sato, *Chem. Lett.*, 2002, **31**, 564–565.